Journal of Materials Chemistry A

ROYAL SOCIETY OF CHEMISTRY

PAPER

View Article Online
View Journal | View Issue

Cite this: J. Mater. Chem. A, 2023, 11, 5584

An efficient polymer acceptor with fluorinated linkers enables all polymer solar cells with an efficiency of 15.7%†

Haiqin Xiao,[a] Junfang Lv,[a] Miao Liu,[a] Xia Guo,[b] Xinxin Xia,[c] Xinhui Lu[c] and Maojie Zhang *[ab]

Received 1st December 2022
Accepted 1st February 2023

DOI: 10.1039/d2ta09364b

rsc.li/materials-a

Despite the significant progress in all-polymer solar cells (all-PSCs) in recent years, obtaining both high open-circuit voltage (V_{OC}) and short-circuit current density (J_{SC}) simultaneously has been a challenging issue. Herein, a novel polymer acceptor PY-DF was developed by polymerizing small molecule acceptor (SMA) monomers with difluorothiophene linkers. Compared to non-fluorinated PYT, PY-DF exhibits a more coplanar and rigid molecular conformation, which leads to better intra-molecular conjugation and enhanced interchain packing, resulting in improved electron mobility and reduced energetic disorder. Furthermore, PY-DF exhibits a relatively up-shifted lowest unoccupied molecular orbital (LUMO) energy level (−3.76 eV) than PYT (−3.80 eV), which is favorable for improving V_{OC}. In addition, the polymer acceptor demonstrates good miscibility with polymer donor, thus leading to optimized phase segregation for superior exciton dissociation and charge transport. As a result, the PY-DF-based all-PSCs achieved a higher PCE of 15.7% with simultaneously enhanced J_{SC} (23.1 mA cm^{-2}) and V_{OC} (0.97 V) in comparison with PYT-based all-PSCs (PCE = 13.2%, J_{SC} = 21.7 mA cm^{-2}, and V_{OC} = 0.93 V). This work provides a promising polymer acceptor for all-PSCs and shows that fluorination of linkers is a potential strategy to build high-performance polymer acceptors.

1. Introduction

Polymer solar cells (PSCs) are considered one of the most promising solar harvesting technologies due to the potential of combining low manufacturing cost, light weight, flexibility, and transparency.[1,2] PSCs based on polymer donors and small molecule acceptors (SMAs) have achieved power conversion efficiencies (PCEs) surpassing 19% to date because of the extensive investigations on efficient photovoltaic materials and device optimization.[3,4] Unlike SMA-based PSCs, all-polymer solar cells (all-PSCs), which comprise conjugated polymers as both donors and acceptors, provide the additional merits of excellent mechanical flexibility, outstanding morphological stability, and great light/thermal stability for large-scale commercialization.[5–7] However, the PCEs of all-PSCs lag behind those of SMA-based PSCs mainly due to the lack of high-performance polymer acceptors.

Before 2017, many classical polymer acceptors had been developed based on naphthalene diimide (NDI),[8] perylene diimide (PDI),[9] bithiophene imide (BTI),[10] B←N-bridged bipyridine (BN-Py),[11] and their derivatives.[12] However, these polymer acceptors usually suffer from some intrinsic flaws such as the weak absorption intensity for NDI-, PDI-, and BTI-based polymer acceptors and the low electron mobility for BN-Py-based polymers, which limit the performance of all-PSCs.[5] Regarding these issues, Li *et al.* creatively proposed a successful strategy by copolymerizing SMAs with π-linkers to construct polymer SMAs (PSMAs).[13] The resulting PSMAs share the same skeleton structure as SMAs and show the advantages of high absorption coefficients, extended photon response, and good crystallinity, which significantly improve the PCEs of all-PSCs.[14,15] Encouraged by the rapid progress of Y-series SMAs,[16,17] researchers in this field have been attracted to using Y-series SMAs to construct high-performance PSMAs.[6,14] Afterwards, many efforts were devoted to further developing PSMAs by modulating π-conjugated fused-ring cores,[18–20] electron-deficient end groups,[21–25] and π-linkers.[26–31] Recently, the PCEs of all-PSCs have reached 18%, narrowing the efficiency gap with SMA-based OSCs.[24,32]

Recent studies have confirmed that the molecular conformations of PSMAs play a crucial role in device

[a]Laboratory of Advanced Optoelectronic Materials, Suzhou Key Laboratory of Novel Semiconductor-optoelectronics Materials and Devices, College of Chemistry, Chemical Engineering and Materials Science, Soochow University, Suzhou 215123, China. E-mail: mjzhang@sdu.edu.cn

[b]National Engineering Research Center for Colloidal Materials, School of Chemistry & Chemical Engineering, Shandong University, Jinan, Shandong 250100, China

[c]Department of Physics, Chinese University of Hong Kong, New Territories, Hong Kong 999077, P. R. China

† Electronic supplementary information (ESI) available. See DOI: https://doi.org/10.1039/d2ta09364b

performance.[23,33,34] For example, the commonly used thiophene linkers contribute to twisted molecular conformations and "randomness" to the polymer backbone, which negatively impact the properties of polymers.[27,34] Yu *et al.* reported a vinyl linker-based polymer PY-V-γ, which exhibits a more coplanar and rigid molecular conformation leading to tighter interchain packing and higher mobility.[27] Therefore, the PY-V-γ-based device shows simultaneously enhanced J_{SC} (24.75 mA cm^{-2}) and fill factor (FF = 75.8%) than those of PM6 : PY-T-γ (J_{SC} = 24.1 mA cm^{-2} and FF = 71.9%). However, the PY-V-γ-based device exhibits a lower V_{OC} (0.91 V) than that based on PYT (0.93 V) due to the downshifted lowest unoccupied molecular orbital (LUMO) level of PY-V-γ.[27] Furthermore, severe phase separation morphology is observed in all-PSCs due to reduced entropic contribution of PSMAs relative to SMAs and significantly suppressing the miscibility of donors and acceptors, which is a long-term challenge.[6,14] Therefore, it is essential to take a comprehensive consideration of molecular conformations, energy levels, and microscopic morphology to achieve high V_{OC} and J_{SC} simultaneously in all-PSCs.

Introducing fluorine atoms into polymers is an effective strategy to enhance photovoltaic performance.[35–38] The fluorine atom can effectively enhance the electron affinity of a polymer and facilitate electron transport.[35,39–41] It has been verified that fluorinated end groups can enhance the intramolecular charge transfer (ICT) effect to improve absorption and molecular packing, which ultimately enhance J_{SC} for the corresponding devices.[21,22] Unfortunately, the fluorinated end group strategy results in lower V_{OC} due to the downshifted LUMO levels of acceptors.[21,22,42] Modifying linker units can fine-tune the energy levels and electron transport properties of polymers.[26–28] Previously reported work verified that a difluorothiophene-substituted polymer (BN-2fT) exhibits a slightly up-shifted LUMO level relative to that of nonfluorinated thiophene analogs (BN-T), which contributes to high V_{OC}.[43] Numerous noncovalent interactions have been found in fluorinated polymers, which can increase the planarity of the backbone.[21,35,44] The fluorination strategy can also change the miscibility of donors and acceptors and further fine-tune microscopic morphology.[22,28,45] Therefore, difluoro-substituted thiophenes as linking units of polymer acceptors may provide another effective approach to design high-performance polymer acceptors.

Here we developed a novel polymer acceptor PY-DF by introducing difluorothiophenes as linkers to optimize molecular conformations and optoelectronic properties. PY-DF exhibits more planar molecular conformation and tighter inter-chain stacking, resulting in higher electron mobility (7.56 × 10^{-4} cm^2 V^{-1} S^{-1}) than PYT (1.68 × 10^{-4} cm^2 V^{-1} s^{-1}). Furthermore, the up-shifted LUMO level (−3.76 eV) for PY-DF in comparison with that of PYT (−3.80 eV) can contribute to increasing the V_{OC} of the resulting devices. In addition, the fluorination effect improves the miscibility of the donor and acceptor and enables more suitable phase segregation, thus promoting exciton dissociation and charge transport. When blended with PM6, the PY-DF-based device showed a higher PCE of 15.7% with simultaneously enhanced V_{OC} (0.97 V), J_{SC} (23.1 mA cm^{-2}), and FF (70.2%) in comparison with the PM6 : PYT-based device (PCE = 13.2%, V_{OC} = 0.93 V, J_{SC} = 21.7 mA cm^{-2}, and FF = 65.6%).

2. Results and discussion

2.1. Materials synthesis, theoretical calculations and crystalline properties

The synthetic routes of polymer acceptors are shown in Fig. 1a. Both PYT and PY-DF were all synthesized *via* Stille cross-coupling polymerization of Y5–C20–Br (M1) and 2,5-bis(trimethylstannyl)thiophene (M2) or (3,4-difluorothiophene-2,5-diyl)bis(trimethylstannane) (M3). The synthetic routes are detailed in the ESI.† The two polymers can be readily dissolved in common solvents including chlorobenzene (CB), toluene (Tol), and chloroform (CF). As measured by gel permeation chromatography (GPC), the PYT and PY-DF acceptors exhibit comparable number average molecular weights (M_n)/polydispersity index (PDI) of 10.1 kDa/1.7 and 10.0 kDa/1.8, respectively. As shown in Fig. S1,† both polymers show good thermal stability with decomposition temperature (T_d, 5% weight loss) above 300 °C under a nitrogen atmosphere.

Density functional theory (DFT) calculations of Gaussian simulation at the B3LYP/631G(d,p) level were carried out to study the impact of linkers on molecular geometry. All alkyl chains were replaced by methyl groups to simplify DFT calculations. For PY-DF, there is an obvious noncovalent C–F···H interaction effect between H atoms on end groups and F atoms on difluorothiophene linkers (Fig. 1b), which facilitates obtaining excellent backbone coplanarity.[35,44] Compared to PYT with dihedral angles of 17.51° and 18.51° between the end group and adjacent thiophene linker and 2.04° between the end group and adjacent BTTP unit, PY-DF shows smaller dihedral angles between the end group and adjacent difluorothiophene linker (11.97° and 12.65°) and between the end group and adjacent BTTP unit (1.03°). The enhanced molecular planarity of PY-DF compared to PYT is beneficial for interchain packing and charge transport.[21,27,46]

The molecular orientations and packing of neat films were investigated by grazing incident wide-angle X-ray diffraction (GIWAXS) measurements and the corresponding results are exhibited in Fig. 1d and e, and Table S1.† Both PY-DF and PYT neat films display quite similar stacking behaviors with preferred "face-on" packing. The PY-DF film displays a smaller π–π stacking spacing (*d*-spacing) of 3.81 Å with a higher crystal coherence length (CCL) of 18.85 Å compared to the PYT film (*d*-spacing = 3.85 Å and CCL = 16.15 Å) in the out-of-plane (OOP) direction. In addition, the CCL value in the in-plane (IP) direction for PY-DF (CCL = 28.27 Å) is higher than that of PYT (20.19 Å). The higher CCLs for PY-DF than PYT in both π–π stacking in the OOP direction and lamellar stacking in the IP direction indicate that PY-DF exhibits more ordered intermolecular packing and strong crystallization propensity, which is favorable for charge transport.[46] The charge carrier mobilities of PY-DF and PYT films were measured by the space-charge-limited current (SCLC) method. The electron mobility (μ_e) for the PY-

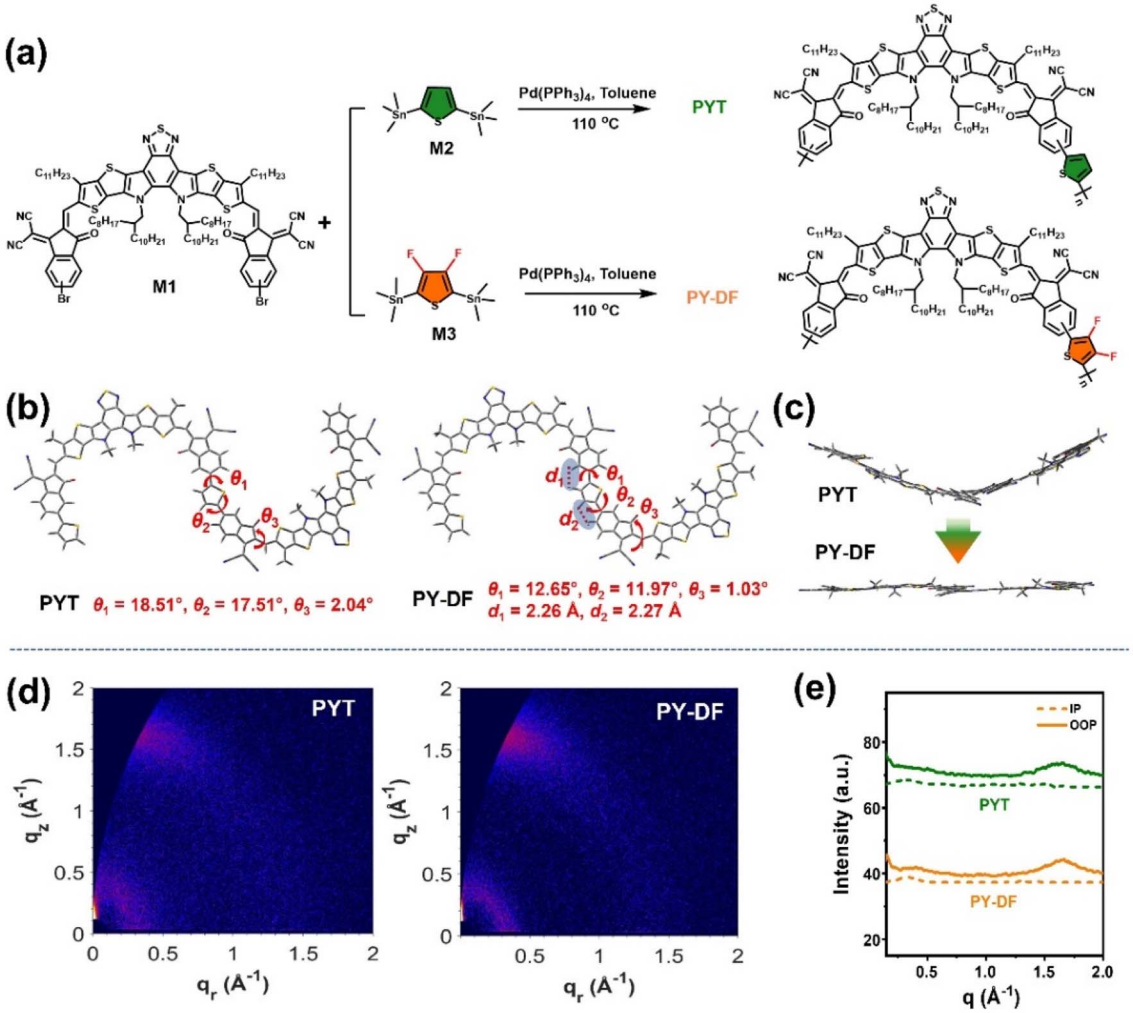

Fig. 1 (a) The synthetic routes and molecular structures of monomers and polymer acceptors. Simulated chemical geometry from DFT calculations: (b) top-view and (c) side-view of PYT and PY-DF. (d) The 2D GIWAXS patterns and (e) the corresponding in-plane (IP) and out-of-plane (OOP) line cuts of neat films.

DF neat film (7.56×10^{-4} cm^2 V^{-1} s^{-1}) is higher than that of PYT (1.68×10^{-4} cm^2 V^{-1} s^{-1}), probably mainly due to the stronger crystallization propensity and intermolecular interaction of PY-DF (Fig. S2†).[47]

2.2. Optical and electrochemical properties

The ultraviolet-visible-near-infrared (UV-vis-NIR) absorption spectra of PYT and PY-DF in chloroform solution and thin films are shown in Fig. 2a and b, respectively. In solution, PY-DF shows a blue-shifted maximum absorption peaks ($\lambda_{max,sol}$ = 740 nm) relative to that of PYT (779 nm), which can be ascribed to the weaker ICT induced by difluorothiophene linkers.[43] In thin films, PY-DF and PYT display similar maximum absorption peaks ($\lambda_{max,film}$) at 792 and 794 nm, respectively, while PY-DF exhibits a broader absorption range. PY-DF shows an obvious red-shift (52 nm) from solutions to films while PYT exhibits a smaller red-shift (15 nm), implying the enhanced molecular packing feature of PY-DF.[42] The optical bandgaps (E_g^{opt}) of PY-DF and PYT are 1.43 and 1.40 eV, respectively, calculated from absorption onsets in films. As shown in Fig. 2b, the maximum extinction coefficient ($\alpha_{max,film}$) increases from 1.11×10^5 cm^{-1} of the PYT film to 1.21×10^5 cm^{-1} of the PY-DF film, which might favor photon utilization and facilitate higher J_{SC} in the corresponding all-PSCs. As shown in Fig. 2c and Fig. S3,† PY-DF exhibits a comparable highest occupied molecular orbital (HOMO) level (−5.68 eV) to PYT (−5.67 eV). However, the LUMO level of PY-DF (−3.76 eV) is slightly higher than that of PYT (−3.80 eV) by the cyclic voltammetry (CV) method, which facilitates higher V_{OC} for the corresponding devices.

2.3. Photovoltaic performance of all-PSCs

All-PSCs were fabricated with a conventional device structure of ITO/PEDOT : PSS/active layer/PFN-Br/Ag. The photovoltaic properties were optimized by changing D/A weight ratios, adjusting thermal annealing (TA) temperature, and adding solvent additives (Fig. S4; Tables S2–S4†). The optimal current density–voltage (J–V) curves are plotted in Fig. 3a, and the detailed photovoltaic parameters are collected in Table 1. The

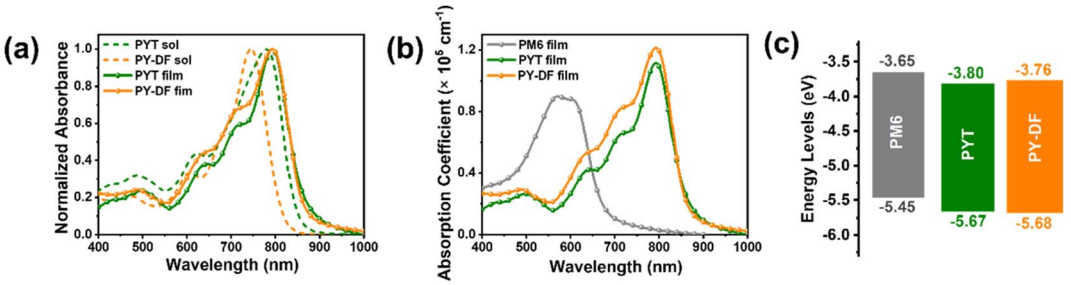

Fig. 2 (a) Normalized UV-vis-NIR absorption spectra of PYT and PY-DF in solution and as thin films. (b) Absorption coefficient of PM6, PYT and PY-DF films. (c) Energy level diagram of PM6, PYT, and PY-DF.

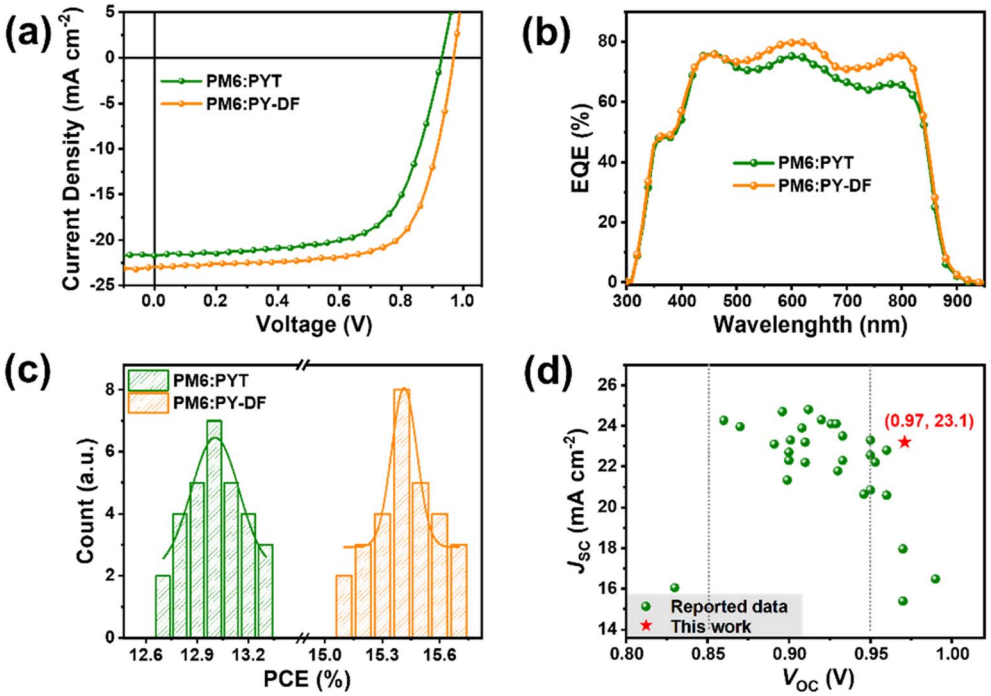

Fig. 3 (a) J–V curves of optimal devices based on PM6 : PYT and PM6 : PY-DF. (b) EQE curves of the corresponding devices. (c) Histograms of the PCE measurements for over 30 individual PM6 : PYT, and PM6 : PY-DF-based devices. (d) Plots of J_{SC} against V_{OC} for binary all-PSCs reported previously with PCEs of over 9% and this work.

PM6 : PYT-based device yields a V_{OC} of 0.93 V, a J_{SC} of 21.7 mA cm^{-2}, and a FF of 65.6%, resulting in a PCE of 13.2%. As expected, the PM6 : PY-DF-based device shows a higher V_{OC} of 0.97 V (~40 mV higher than that of the PYT-based device), which may benefit from the high-lying LUMO level of PY-DF and reduced E_{loss} (discussed below). Compared to the PM6 : PYT-based device, the PM6 : PY-DF-based device exhibits higher J_{SC} (23.1 mA cm^{-2}) and FF (70.2%), which may result from optimized blend morphology. Therefore, a high PCE of 15.7% can be achieved in PM6 : PY-DF-based devices. These two devices both have over 70% external quantum efficiency (EQE) in the absorption region of 450–850 nm, while the overall EQE values (the maximum is close to 80%) of the PY-DF-based device are much higher than those of the PYT-based device (Fig. 3b). The calculated integrated J_{SC} value of the PM6 : PY-DF device (22.1 mA cm^{-2}) is higher than that of PM6 : PYT (20.9 mA cm^{-2}). Fig. 3c shows a histogram of PCEs for PM6 : PYT and PM6 : PY-DF devices of 30 independent cells and shows Gaussian distribution, indicating good reproducibility of photovoltaic performance in the corresponding all-PSCs. Fig. 3d and Table S5† summarize the key device parameters for representative high-efficiency binary all-PSCs. To the best of our knowledge, the V_{OC} value in this work is one of the highest among those of binary all-PSCs with a J_{SC} exceeding 18 mA cm^{-2}. The simultaneous enhancements in V_{OC}, J_{SC} and FF from PY-DF-based devices indicate that difluorothiophenes as linkers are very meaningful for molecular design of PSMAs.

2.4. Exciton dissociation, and charge recombination and transport

As shown in Fig. 4a and S5,† the PM6 : PY-DF-based blends show higher and more balanced charge carrier mobilities (hole

Table 1 Photovoltaic parameters of all-PSCs based on PM6 : acceptors (1 : 1, w/w) under AM 1.5 G illumination (100 mW cm^{-2})

Active layers	V_{OC}[a] (V)	J_{SC}[a] (mA cm^{-2})	Cal. J_{SC}[b] (mA cm^{-2})	FF[a] (%)	PCE[a] (%)
PM6 : PYT	0.93 (0.92 ± 0.01)	21.7 (21.5 ± 0.2)	20.9	65.6 (64.4 ± 1.2)	13.2 (12.9 ± 0.3)
PM6 : PY-DF	0.97 (0.96 ± 0.01)	23.1 (22.9 ± 0.2)	22.1	70.2 (69.1 ± 1.1)	15.7 (15.4 ± 0.3)

[a] The mean values and standard deviations of device parameters based on 30 devices are shown in parentheses. [b] The integral J_{SC} from EQE curves.

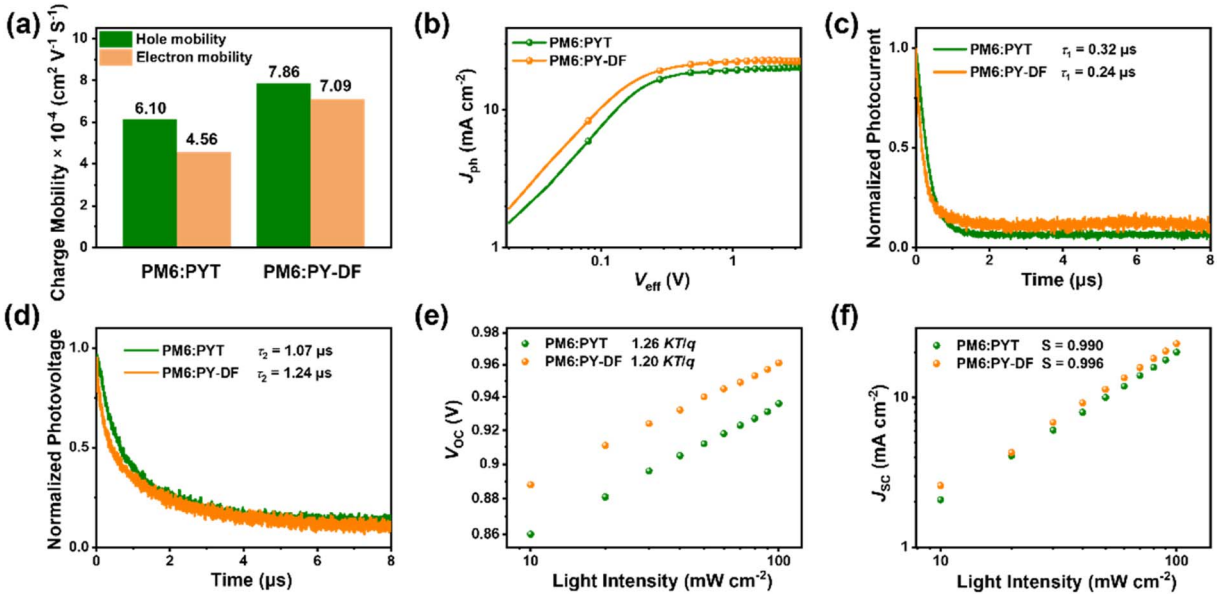

Fig. 4 (a) Hole and electron mobilities. (b) The plots of J_{ph} *versus* V_{eff} curves of PM6 : PYT and PM6 : PY-DF all-PSCs. (c) TPC and (d) TPV measurements. (e) and (f) The dependence of V_{OC} and J_{SC} on P_{light} of the corresponding all-PSCs.

mobilities, $\mu_h = 7.86 \times 10^{-4}$ cm^2 V^{-1} s^{-1}, $\mu_e = 7.09 \times 10^{-4}$ cm^2 V^{-1} s^{-1}, and $\mu_h/\mu_e = 1.11$) than PM6 : PYT-based blends ($\mu_h = 6.10 \times 10^{-4}$ cm^2 V^{-1} s^{-1}, $\mu_e = 4.56 \times 10^{-4}$ cm^2 V^{-1} s^{-1}, and $\mu_h/\mu_e = 1.34$). More balanced charge transport for PM6 : PY-DF can minimize the impact of space-charge formation and high mobility charge carriers can be transported to the electrode more quickly, contributing to higher J_{SC} and FF.[48] To understand the exciton dissociation and charge collection process, the photocurrent density (J_{ph}) *versus* effective voltage (V_{eff}) of PYT and PY-DF-based devices were investigated and are shown in Fig. 4b. The V_{eff} is obtained from $V_{eff} = V_{OC} - V_{app}$, where V_{app} is applied voltage.[47,49] The values of exciton dissociation probability (P_{diss}) and charge collection probability (P_{coll}) for PM6 : PY-DF and PM6 : PYT were calculated to be 98.2%/84.5% and 96.5%/79.5% under the short-circuit and maximum power output conditions, respectively. Obviously, the PM6 : PY-DF devices show the more efficient processes of exciton dissociation and charge collection. Photoluminescence (PL) was recorded to further study exciton dissociation and charge transfer behavior of PY-DF and PYT neat films and their blends. As shown in Fig. S6,† compared to PL spectra of PM6 and PYT neat films, more than 99.3% and 83.8% of PL quenching for the donor and acceptor, respectively, can be achieved for PM6 : PYT blends. Notably, the PM6 : PY-DF blends show higher PL quenching of over 99.8% and 85.9% for the donor and acceptor, respectively, meaning more effective charge transfer between PM6 and PY-DF.[50]

Transient photocurrent (TPC) measurement was also performed to evaluate the charge carrier generation and transportation properties. As shown in Fig. 4c, the photocurrent decay times (τ_1) of PM6 : PYT, and PM6 : PY-DF were determined to be 0.32 and 0.24 μs, respectively. The shorter extraction lifetime suggests that the PM6 : PY-DF device has a faster charge sweep-out and a superior charge extraction capacity than PM6 : PYT devices. In addition, transient photovoltage (TPV) measurement was performed to evaluate the recombination rate of charge carriers in all-PSCs (Fig. 4d). The PY-DF-based device shows a higher charge carrier lifetime (τ_2) than the PYT-based device, indicating less carrier recombination, mainly attributed to the more balanced carrier mobility and reduced charge trap states. The dependence of J_{SC} and V_{OC} on light intensity (P_{light}) was investigated to analyze charge recombination behavior. As shown in Fig. 4e, the $V_{OC} - P_{light}$ measurements reveal that the slope of the PM6 : PYT device (1.26 kT/q) is higher than that of the PM6 : PY-DF device (1.20 kT/q), suggesting that trap-assisted recombination of charge carriers in the PM6 : PYT device is more significant than in the PY-DF-based device.[51] The P_{light} dependence of J_{SC} demonstrated the weaker bimolecular recombination in the PM6 : PY-DF device ($S = 0.996$) than the PM6 : PYT device ($S = 0.990$), which can be calculated using the power-law equation $J_{SC} \propto P_{light}^{S}$ (where S is an exponential constant) (Fig. 4f).[52] All results

are well consistent with the higher J_{SC} and FF in PY-DF-based all-PSCs.

2.5. Energy loss

To gain insight into the higher V_{OC} delivered by PM6 : PY-DF devices, the E_{loss} characteristic was explored *via* Fourier transform photocurrent spectroscopy (FTPS–EQE) and electroluminescence external quantum efficiency (EQE_{EL}) spectra (Fig. S7† and Table 2).[27] According to detailed balance theory, the energy loss can be described by the following equation:[53]

$$E_{loss} = (E_g^{PV} - qV_{OC,SQ}) + (qV_{OC,SQ} - qV_{OC,Rad}) + (qV_{OC,Rad} - qV_{OC}) = \Delta E_1 + \Delta E_2 + \Delta E_3$$

where E_g^{PV} is the optical gap (E_g^{PV}), q is the elementary charge, $V_{OC,SQ}$ is the maximum voltage by the Shockley–Queisser limit, and $V_{OC,Rad}$ is open-circuit voltage considering only radiative recombination.[54] It is widely known that ΔE_1 is inevitable in OSCs and correlated to radiative recombination above the E_g^{PV}.[48] As shown in Fig. S7a and b,† E_g^{PV} of PM6 : PYT and PM6 : PY-DF blends were calculated to be ~1.45 eV. Both devices show the same ΔE_1 value of 0.26 eV. ΔE_2 and ΔE_3 are caused by radiative recombination below the gap and non-radiative recombination, respectively.[25] Compared with the PM6 : PYT device (ΔE_2 = 0.04 eV), the PM6 : PY-DF device shows a slight reduction of ΔE_2 (0.02 eV). ΔE_3 can be directly estimated from EQE_{EL} spectra using the equation: $\Delta E_3 = -KT \ln EQE_{EL}$.[50] As shown in Fig. S7d,† the PM6 : PY-DF device exhibits higher EL emission and produces lower EQE_{EL}, and finally shows a lower ΔE_3 value (0.20 eV) than the PM6 : PYT device (ΔE_3 = 0.22 eV). The total E_{loss} values are determined to be 0.48 and 0.52 eV for PM6 : PY-DF and PM6 : PYT, respectively, and the reduced E_{loss} in PY-DF-based all-PSCs is mainly attributable to the lower ΔE_2 and ΔE_3 values (Fig. 5a).

The urbach energy (E_U) values were further calculated from the exponential tail near the band edge of the corresponding FTPS–EQE spectra (Fig. S7c†) using the following equation:[55]

$$\ln EQE = c + \frac{hv}{E_U}$$

where c is a constant and hv is photon energy. E_U is urbach energy, which is often represented as energetic disorder and correlated to non-radiative recombination.[55–57] The PY-DF-based device exhibits an E_U of 21.73 meV, which is significantly lower than that of the PYT-based device (25.80 meV). The low E_U of PY-DF benefits the decreased E_{loss} in the corresponding devices and is attributed to the more planar molecular conformation and enhanced intermolecular packing of PY-DF.[27] These results suggest that reduced E_{loss} and E_U values are the major reasons for the high V_{OC} of PY-DF-based devices. Fig. 5b summarizes the correlation of eV_{OC} against E_g^{PV} in this work in comparison with other binary all-PSCs (PCE > 9%) based on representative polymer acceptors. Most all-PSCs show E_{loss} of over an empirical threshold of 0.5 eV and only a few systems could maximize the V_{OC} and minimize the E_{loss} values. The V_{OC} in our work is among the highest values for PSCs with an E_{loss} below 0.5 meV. The correlation of PCE against $E_g - eV_{OC}$ is shown in Fig. 5c. The optimal photovoltaic parameters for PM6 : PY-DF-based devices are both high PCE and low $E_g - eV_{OC}$ simultaneously. The results indicate that introducing the difluorothiophenes as linkers in PSMAs is one of the most effective ways to achieve a high V_{OC} with low E_{loss} values.

2.6. Film morphology

To investigate the fluorination effect on blend film morphology, atomic force microscopy (AFM) and transmission electron microscopy (TEM) were carried out. As shown in Fig. 6a and b, both blends display distinct uniform and fibrillar bicontinuous

Table 2 Detailed E_{loss} of the PM6 : PYT and PM6 : PY-DF based devices

Active layer	V_{OC}[a] (V)	E_g^{PV}[b] (eV)	E_{loss}[c] (eV)	EQE_{EL}[d] (%)	ΔE_1 (eV)	ΔE_2 (eV)	ΔE_3 (eV)
PM6 : PYT	0.93	1.45	0.52	1.67×10^{-2}	0.26	0.04	0.22
PM6 : PY-DF	0.97	1.45	0.48	3.87×10^{-2}	0.26	0.02	0.20

[a] The V_{OC} values were calculated from J–V curves. [b] The E_g^{PV} values were determined from derivatives of EQE spectra. [c] E_{loss} is equal to the difference between E_g^{PV} and V_{OC}. [d] EQE_{EL} is EL quantum efficiency.

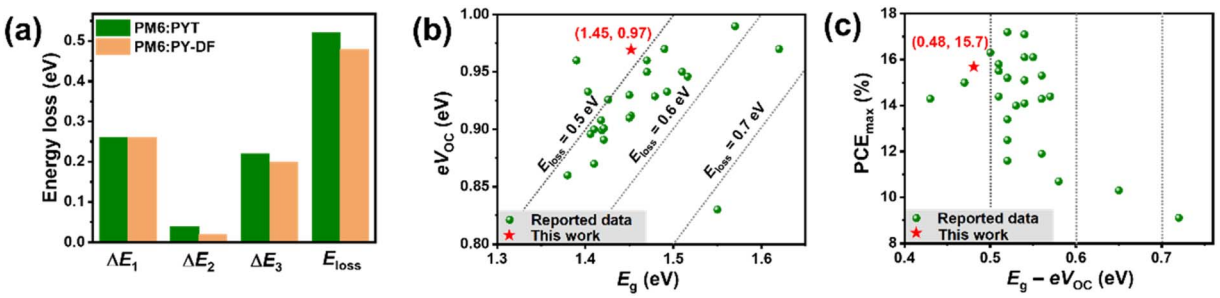

Fig. 5 (a) E_{loss} and its detailed three part values (ΔE_1, ΔE_2, and ΔE_3) of PM6 : PYT and PM6 : PY-DF-based devices. (b) Plots of eV_{OC} against E_g^{PV} and (c) PCE against $E_g - eV_{OC}$ in all-PSCs with PCEs of over 9% reported in the literature.

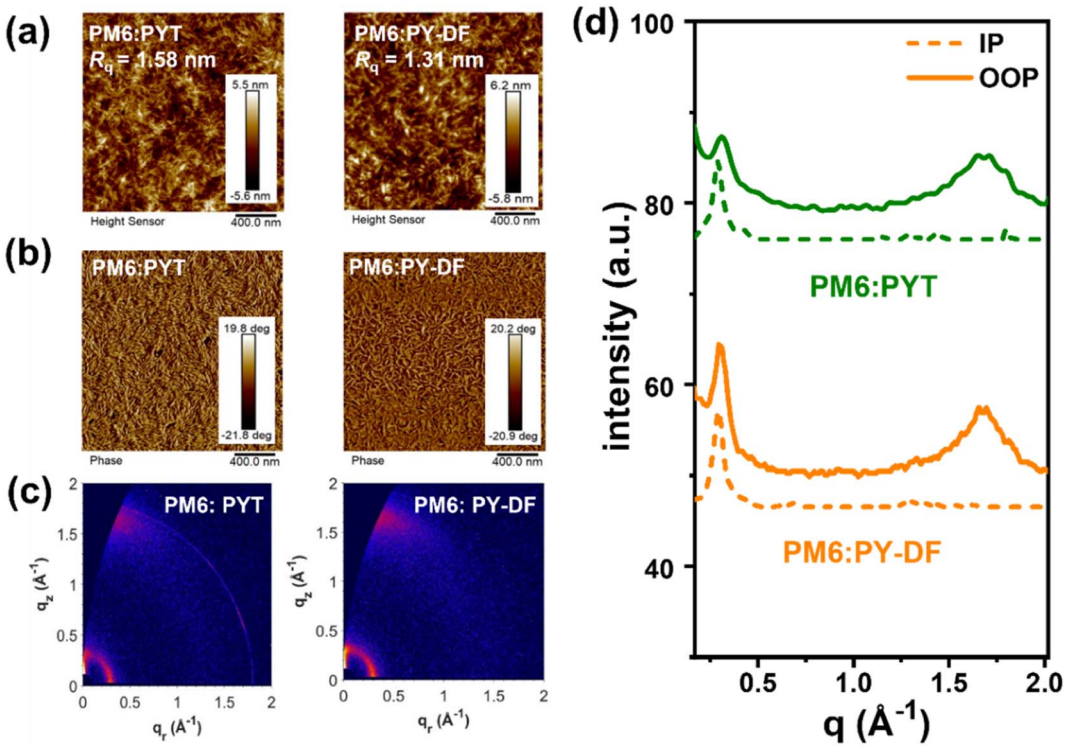

Fig. 6 The AFM (a) height images and (b) phase images. (c) The 2D GIWAXS profiles and (d) the corresponding IP and OOP line-cuts of blend films.

interpenetrating networks. The PM6 : PYT films show a relatively coarse surface with a root-mean-square surface roughness (R_q) value of 1.58 nm. By contrast, the PM6 : PY-DF films demonstrate a uniform and relatively smooth surface with a R_q of 1.31 nm, facilitating efficient exciton separation, charge transfer and extraction.[28] Furthermore, the TEM results demonstrate that delicate bright and dark regimes could be clearly observed in PM6 : PY-DF films (Fig. S8b†), while large size bright regimes are shown in PM6 : PYT films (Fig. S8a†). Unlike the larger phase separation of PM6 : PYT, the suitable phase separation of PM6 : PY-DF provides more donor–acceptor interfaces for efficient charge dissociation.[40] Contact angle measurements were further performed to explore the fundamental origin of the morphological difference. As shown in Fig. S9 and Table S6,† the surface energy (γ) of PM6 was calculated to be 31.25 mN m^{-1} using the Wu method.[58,59] For PSMAs, PY-DF (38.73 mN m^{-1}) shows a lower γ value than PYT (40.82 mN m^{-1}). Furthermore, the miscibility of PM6 with the two polymer acceptors was evaluated using Flory–Huggins interaction parameters (χ).[50] The χ between PM6 and PY-DF was calculated to be 0.40, which is lower than 0.64 for PM6/PYT. The weaker interaction between PM6 and PY-DF indicates better miscibility, and thus a relatively small and suitable domain size in blends, which is consistent with the TEM results.[22]

The crystalline nature and molecular packing of blend films were investigated by GIWAXS measurements. Fig. 6c and d show the 2D patterns and the relevant crystallographic parameters are shown in Table S7.† Both blends show sharp (010) π–π stacking diffraction peaks in the OOP direction, which exhibits a clear "face-on" dominant orientation. For the (010) peaks in the OOP direction, the PM6 : PY-DF blend exhibits smaller *d*-spacing and higher coherence lengths (3.74 Å and 23.56 Å at 1.67 Å^{-1}) compared to the PM6 : PYT blend (3.78 Å and 21.74 Å at 1.66 Å^{-1}). The CCL in the IP direction also increases from 23.56 Å for the PM6 : PYT blend to 25.70 Å for the PM6 : PY-DF blend, indicating the improved crystallite size in PM6 : PY-DF blends. These above results explain the reason why the charge mobility is higher for PY-DF than for PYT, which eventually results in higher J_{SC} and FF for PM6 : PY-DF-based all-PSCs.

3. Conclusion

In summary, we designed and synthesized a novel polymer acceptor PY-DF with difluorothiophenes as linkers for all-PSC fabrications. The C–F···H noncovalent interaction between the difluorothiophene linkers and end groups results in more planar and rigid molecular conformation than that of PYT based on thiophene linkers. Therefore, PY-DF displays enhanced electron mobility, molecular crystallinity, and reduced energy disorder. In addition, PY-DF exhibits a lower surface energy than nonfluorinated PYT, leading to improved miscibility with PM6. The increased crystallinity and miscibility enable PM6 : PY-DF to achieve an optimized active layer morphology, facilitating charge separation and transport. PY-DF exhibits up-shifted LUMO levels than PYT, leading to higher V_{OC} in all-PSCs. As a result, PM6 : PY-DF-based all-PSCs achieved an optimal PCE of 15.7% with both high V_{OC} (0.97 V) and J_{SC} (23.1 mA cm^{-2}), corresponding to a ~19% improvement

in the PCE of the PM6 : PYT-based device. To the best of our knowledge, this value of V_{OC} is one of the highest among all-PSCs. This study indicates that fluorination of linker units is a potential strategy to build high-performance polymer acceptors for all-PSC application.

Conflicts of interest

There are no conflicts of interest to declare.

Acknowledgements

This work was supported by the National Natural Science Foundation of China (NSFC) (No. 51973146), the Shandong Provincial Natural Science Foundation for Distinguished Young Scholars (ZR2022JQ09), and the Collaborative Innovation Center of Suzhou Nano Science & Technology. Grazing-incidence wide-angle X-ray scattering (GIWAXS) measurements were carried out with a Xeuss 2.0 SAXS/WAXS laboratory beamline using a Cu X-ray source, which is supported by the Department of Physics, Chinese University of Hong Kong.

References

1 J. Wang, P. Xue, Y. Jiang, Y. Huo and X. Zhan, *Nat. Rev. Chem.*, 2022, **6**, 614–634.
2 A. Wadsworth, M. Moser, A. Marks, M. S. Little, N. Gasparini, C. J. Brabec, D. Baran and I. McCulloch, *Chem. Soc. Rev.*, 2019, **48**, 1596–1625.
3 W. Gao, F. Qi, Z. Peng, F. R. Lin, K. Jiang, C. Zhong, W. Kaminsky, Z. Guan, C. S. Lee, T. J. Marks, H. Ade and A. K. Jen, *Adv. Mater.*, 2022, **34**, 2202089.
4 L. Zhu, M. Zhang, J. Xu, C. Li, J. Yan, G. Zhou, W. Zhong, T. Hao, J. Song, X. Xue, Z. Zhou, R. Zeng, H. Zhu, C. C. Chen, R. C. I. MacKenzie, Y. Zou, J. Nelson, Y. Zhang, Y. Sun and F. Liu, *Nat. Mater.*, 2022, **21**, 656–663.
5 C. Lee, S. Lee, G. U. Kim, W. Lee and B. J. Kim, *Chem. Rev.*, 2019, **119**, 8028–8086.
6 G. Wang, A. F. Ferdinand, S. Melkonyan and T. J. Marks, *Angew. Chem., Int. Ed.*, 2019, **58**, 4129–4142.
7 Z. Genene, W. Mammo, E. Wang and M. R. Andersson, *Adv. Mater.*, 2019, **31**, 1807275.
8 X. Guo, A. Facchetti and T. J. Marks, *Chem. Rev.*, 2014, **114**, 8943–9021.
9 Q. Shi, J. Wu, X. Wu, A. Peng and H. Huang, *Chem.–Eur. J.*, 2020, **26**, 12510–12522.
10 K. Feng, H. Guo, H. Sun and X. Guo, *Acc. Chem. Res.*, 2021, **54**, 3804–3817.
11 R. Zhao, J. Liu and L. Wang, *Acc. Chem. Res.*, 2020, **53**, 1557–1567.
12 J. Yang, B. Xiao, A. Tang, J. Li, X. Wang and E. Zhou, *Adv. Mater.*, 2019, **31**, 1804699.
13 Z. G. Zhang, Y. Yang, J. Yao, L. Xue, S. Chen, X. Li, W. Morrison, C. Yang and Y. Li, *Angew. Chem., Int. Ed.*, 2017, **56**, 13503–13507.
14 B. Wu, B. Yin, C. Duan and L. Ding, *J. Semicond.*, 2021, **42**, 080301.
15 S. Ma, H. Zhang, K. Feng and X. Guo, *Chem.–Eur. J.*, 2022, **28**, 202200222.
16 J. Yuan, Y. Zhang, L. Zhou, G. Zhang, H.-L. Yip, T.-K. Lau, X. Lu, C. Zhu, H. Peng, P. A. Johnson, M. Leclerc, Y. Cao, J. Ulanski, Y. Li and Y. Zou, *Joule*, 2019, **3**, 1140–1151.
17 C. Li, J. Zhou, J. Song, J. Xu, H. Zhang, X. Zhang, J. Guo, L. Zhu, D. Wei, G. Han, J. Min, Y. Zhang, Z. Xie, Y. Yi, H. Yan, F. Gao, F. Liu and Y. Sun, *Nat. Energy*, 2021, **6**, 605–613.
18 X. Gu, Y. Wei, X. Liu, N. Yu, L. Li, Z. Han, J. Gao, C. Li, Z. Wei, Z. Tang, X. Zhang and H. Huang, *Sci. China: Chem.*, 2022, **65**, 926–933.
19 H. Fu, Y. Li, J. Yu, Z. Wu, Q. Fan, F. Lin, H. Y. Woo, F. Gao, Z. Zhu and A. K. Jen, *J. Am. Chem. Soc.*, 2021, **143**, 2665–2670.
20 W. Wang, Q. Wu, R. Sun, J. Guo, Y. Wu, M. Shi, W. Yang, H. Li and J. Min, *Joule*, 2020, **4**, 1070–1086.
21 F. Peng, K. An, W. Zhong, Z. Li, L. Ying, N. Li, Z. Huang, C. Zhu, B. Fan, F. Huang and Y. Cao, *ACS Energy Lett.*, 2020, **5**, 3702–3707.
22 H. Yu, Z. Qi, J. Yu, Y. Xiao, R. Sun, Z. Luo, A. M. H. Cheung, J. Zhang, H. Sun, W. Zhou, S. Chen, X. Guo, X. Lu, F. Gao, J. Min and H. Yan, *Adv. Energy Mater.*, 2020, **11**, 2003171.
23 Z. Luo, T. Liu, R. Ma, Y. Xiao, L. Zhan, G. Zhang, H. Sun, F. Ni, G. Chai, J. Wang, C. Zhong, Y. Zou, X. Guo, X. Lu, H. Chen, H. Yan and C. Yang, *Adv. Mater.*, 2020, **32**, 2005942.
24 R. Sun, T. Wang, Q. Fan, M. Wu, X. Yang, X. Wu, Y. Yu, X. Xia, F. Cui, J. Wan, X. Lu, X. Hao, A. K. Y. Jen, E. Spiecker and J. Min, *Joule*, 2023, **7**, 221–237.
25 Y. Li, J. Song, Y. Dong, H. Jin, J. Xin, S. Wang, Y. Cai, L. Jiang, W. Ma, Z. Tang and Y. Sun, *Adv. Mater.*, 2022, **34**, 2110155.
26 H. Sun, B. Liu, Y. Ma, J. W. Lee, J. Yang, J. Wang, Y. Li, B. Li, K. Feng, Y. Shi, B. Zhang, D. Han, H. Meng, L. Niu, B. J. Kim, Q. Zheng and X. Guo, *Adv. Mater.*, 2021, **33**, 2102635.
27 H. Yu, Y. Wang, H. K. Kim, X. Wu, Y. Li, Z. Yao, M. Pan, X. Zou, J. Zhang, S. Chen, D. Zhao, F. Huang, X. Lu, Z. Zhu and H. Yan, *Adv. Mater.*, 2022, **34**, 2200361.
28 D. Zhou, C. Liao, S. Peng, X. Xu, Y. Guo, J. Xia, H. Meng, L. Yu, R. Li and Q. Peng, *Adv. Sci.*, 2022, **9**, 2202022.
29 Q. Fan, Q. An, Y. Lin, Y. Xia, Q. Li, M. Zhang, W. Su, W. Peng, C. Zhang, F. Liu, L. Hou, W. Zhu, D. Yu, M. Xiao, E. Moons, F. Zhang, T. D. Anthopoulos, O. Inganäs and E. Wang, *Energy Environ. Sci.*, 2020, **13**, 5017–5027.
30 Z. Yin, Y. Wang, Q. Guo, L. Zhu, H. Liu, J. Fang, X. Guo, F. Liu, Z. Tang, M. Zhang and Y. Li, *J. Mater. Chem. C*, 2020, **8**, 16180–16187.
31 Y. Wang, N. Wang, Q. Yang, J. Zhang, J. Liu and L. Wang, *J. Mater. Chem. A*, 2021, **9**, 21071–21077.
32 J. Wang, Y. Cui, Y. Xu, K. Xian, P. Bi, Z. Chen, K. Zhou, L. Ma, T. Zhang, Y. Yang, Y. Zu, H. Yao, X. Hao, L. Ye and J. Hou, *Adv. Mater.*, 2022, **34**, 2205009.
33 H. Wang, H. Chen, W. Xie, H. Lai, T. Zhao, Y. Zhu, L. Chen, C. Ke, N. Zheng and F. He, *Adv. Funct. Mater.*, 2021, **31**, 2100877.
34 S. Seo, C. Sun, J. W. Lee, S. Lee, D. Lee, C. Wang, T. N. L. Phan, G. U. Kim, S. Cho, Y. H. Kim and B. J. Kim, *Adv. Funct. Mater.*, 2021, **32**, 2108508.

35 Q. Zhang, M. A. Kelly, N. Bauer and W. You, *Acc. Chem. Res.*, 2017, **50**, 2401–2409.
36 A. Tang, B. Xiao, F. Chen, J. Zhang, Z. Wei and E. Zhou, *Adv. Energy Mater.*, 2018, **8**, 1801582.
37 J. Yang, P. Cong, L. Chen, X. Wang, J. Li, A. Tang, B. Zhang, Y. Geng and E. Zhou, *ACS Macro Lett.*, 2019, **8**, 743–748.
38 T. Dai, X. Li, P. Lei, A. Tang, Y. Geng, Q. Zeng and E. Zhou, *Nano Energy*, 2022, **99**, 107413.
39 K. Kawashima, T. Fukuhara, Y. Suda, Y. Suzuki, T. Koganezawa, H. Yoshida, H. Ohkita, I. Osaka and K. Takimiya, *J. Am. Chem. Soc.*, 2016, **138**, 10265–10275.
40 G. Sun, X. Jiang, X. Li, L. Meng, J. Zhang, S. Qin, X. Kong, J. Li, J. Xin, W. Ma and Y. Li, *Nat. Commun.*, 2022, **13**, 5267.
41 J. W. Jung, J. W. Jo, C. C. Chueh, F. Liu, W. H. Jo, T. P. Russell and A. K. Jen, *Adv. Mater.*, 2015, **27**, 3310–3317.
42 H. Yu, S. Luo, R. Sun, I. Angunawela, Z. Qi, Z. Peng, W. Zhou, H. Han, R. Wei, M. Pan, A. M. H. Cheung, D. Zhao, J. Zhang, H. Ade, J. Min and H. Yan, *Adv. Funct. Mater.*, 2021, **31**, 2100791.
43 Y. Li, H. Meng, T. Liu, Y. Xiao, Z. Tang, B. Pang, Y. Li, Y. Xiang, G. Zhang, X. Lu, G. Yu, H. Yan, C. Zhan, J. Huang and J. Yao, *Adv. Mater.*, 2019, **31**, 1904585.
44 S. Yu, A. Peng, S. Zhang and H. Huang, *Sci. China: Chem.*, 2018, **61**, 1359–1367.
45 J. Wu, C. Y. Liao, Y. Chen, R. M. Jacobberger, W. Huang, D. Zheng, K. W. Tsai, W. L. Li, Z. Lu, Y. Huang, M. R. Wasielewski, Y. M. Chang, T. J. Marks and A. Facchetti, *Adv. Energy Mater.*, 2021, **11**, 2102648.
46 J. Lin, Q. Guo, Q. Liu, J. Lv, H. Liang, Y. Wang, L. Zhu, F. Liu, X. Guo and M. Zhang, *Chin. J. Chem.*, 2021, **39**, 2685–2691.
47 Y. Wang, Y. Wang, L. Zhu, H. Liu, J. Fang, X. Guo, F. Liu, Z. Tang, M. Zhang and Y. Li, *Energy Environ. Sci.*, 2020, **13**, 1309–1317.
48 J. Wu, Q. Fan, M. Xiong, Q. Wang, K. Chen, H. Liu, M. Gao, L. Ye, X. Guo, J. Fang, Q. Guo, W. Su, Z. Ma, Z. Tang, E. Wang, H. Ade and M. Zhang, *Nano Energy*, 2021, **82**, 105679.
49 Y. Ren, X. Liu, H. Li, J. Qin, S. Du, X. Lu, J. Tong, C. Yang and J. Li, *Opt. Mater.*, 2022, **129**, 112520.
50 Q. Guo, J. Lin, H. Liu, X. Dong, X. Guo, L. Ye, Z. Ma, Z. Tang, H. Ade, M. Zhang and Y. Li, *Nano Energy*, 2020, **74**, 104861.
51 L. J. A. Koster, V. D. Mihailetchi, R. Ramaker and P. W. M. Blom, *Appl. Phys. Lett.*, 2005, **86**, 123509.
52 P. Schilinsky, C. Waldauf and C. J. Brabec, *Appl. Phys. Lett.*, 2002, **81**, 3885–3887.
53 J. Yao, T. Kirchartz, M. S. Vezie, M. A. Faist, W. Gong, Z. He, H. Wu, J. Troughton, T. Watson, D. Bryant and J. Nelson, *Phys. Rev. Appl.*, 2015, **4**, 014020.
54 S. Liu, J. Yuan, W. Deng, M. Luo, Y. Xie, Q. Liang, Y. Zou, Z. He, H. Wu and Y. Cao, *Nat. Photonics*, 2020, **14**, 300–305.
55 F. Urbach, *Phys. Rev.*, 1953, **92**, 1324.
56 K. Vandewal, K. Tvingstedt, A. Gadisa, O. Inganäs and J. V. Manca, *Phys. Rev. B: Condens. Matter Mater. Phys.*, 2010, **81**, 125204.
57 C. Zhang, S. Mahadevan, J. Yuan, J. K. W. Ho, Y. Gao, W. Liu, H. Zhong, H. Yan, Y. Zou, S.-W. Tsang and S. K. So, *ACS Energy Lett.*, 2022, **7**, 1971–1979.
58 S. Nilsson, A. Bernasik, A. Budkowski and E. Moons, *Macromolecules*, 2007, **40**, 8291–8301.
59 L. Xue, X. Liu, Q. Wang, M. Yang, S. Du, C. Yang, J. Tong, Y. Xia and J. Li, *Energy Technol.*, 2022, **10**, 2200504.